Interstitial micelles in binary blends of *ABA* triblock copolymers and homopolymers

S. Wołoszczuk[1] and M. Banaszak[1,2,*]

[1]*Faculty of Physics, A. Mickiewicz University, ul. Umultowska 85, 61-614 Poznan, Poland*

[2]*NanoBioMedical Centre, Adam Mickiewicz University, ul. Umultowska 85, 61-614 Poznan, Poland*

(Received 3 September 2017; published 17 January 2018)

We investigate triblock-homopolymer blends of types A1BA2/A and A1BA2/B, using a lattice Monte Carlo method. While the simulated triblock chains are compositionally symmetric in terms of the A-to-B volume ratio, the A1 block is significantly shorter than the A2 block. For the pure A1BA2 melt and the A1BA2 solutions in selective solvent the phase behavior is relatively well known, including existence and stability of the interstitial micelles which were discovered in previous Monte Carlo simulations. In this paper we study the stability of the interstitial micelles as a function of triblock volume fraction in selective homopolymers of either type A or type B, using two significantly different homopolymer chain lengths. We found that adding selective homopolymer of type A shifts the stability of the interstitial micelles into significantly higher temperatures. We also obtained, via self-assembly, intriguing new nanostructures which can be identified as ordered truncated octahedra. Finally, we established that the phase behavior of the triblock-homopolymer blends depends relatively weakly on the chain length of the added homopolymer.

DOI: 10.1103/PhysRevE.97.012503

I. INTRODUCTION

Block copolymers are extensively studied due to their intrinsic ability to self-organize spontaneously into a plethora of periodic nanostructures, to compatibilize immiscible polymers, and to locate at polymer-polymer interfaces [1–12]. These intriguing soft materials can form nanostructures on microphase separation which occurs via an order-disorder transition (ODT). Furthermore, order-order transitions (OOT) are observed between different self-assembled morphologies. In this paper, we focus our attention exclusively on model ABA triblock-homopolymers blends by extending the scope previous papers [13,14] and aiming at a new goal.

In a previous paper [13], we examined pure triblock melts, employing lattice Monte Carlo simulations and, selectively, dissipative particle dynamics. We explored the phase behavior of molecularly asymmetric A1BA2 copolymers possessing chemically identical endblocks (A1 and A2) but differing significantly in length. In the limit of superstrong segregation, interstitial micelles (IM) composed of the minority $A1$ endblock were observed to arrange into two-dimensional hexagonal arrays along the midplane of B-rich lamellae in compositionally symmetric (50:50 A:B) copolymers. Simulations established the molecular asymmetry and incompatibility conditions under which such micelles formed, as well as the temperature dependence of their aggregation number. Beyond an optimal length of the $A1$ endblock, the propensity for interstitial micelles (IM) to develop decreased, and the likelihood for collocation of both endblocks in the $A2$-rich lamellae increased. Moreover, in pure triblock melts, the IM's were stable at very strong segregations which correspond to either very low temperatures or very long chains. Note that short A blocks should not be present in the B-matrix due to enthalpic penalty originating from the increased number of A-B contacts. However, due to an entropic gain originating from an increased number of available locations, the short A blocks can be localized in the B matrix [15].

Moreover, we found [14] that adding selective solvent of type A shifts the stability of the IM's into significantly higher temperatures which may provide a pathway towards experimental studies of interstitial micelles in real triblock solutions, such as, for example, polystyrene-polyisoprene-polystyrene triblock. We also found that adding selective solvent (either A or B) gives rise a to more complex phase behavior with the nanodomains ordered into a variety of nonlamellar morphologies for temperatures and compositions at which the IM's are stable.

In this paper, we study the A1BA2-homopolymer blends in selective homopolymer of either type A or B, using two different homopolymer chain lengths (N_H): $N_H = \frac{1}{4}N_C$ and $N_H = N_C$, where N_C is the copolymer chain length.

II. MODEL AND METHOD

The cooperative motion algorithm (CMA) [16–21], based on the FCC lattice, is used to simulate the triblock solutions and blends. The FCC lattice is a reasonably good choice as far as the number of nearest neighbors is concerned ($z = 12$) because in dense simple liquids this number is also close to 12. We did perform simulation on the cubic lattice ($z = 6$) [22] and off-lattice [23] for single copolymer chains and the results did not differ qualitatively from those on the FCC lattice.

We apply standard Monte Carlo (MC) simulations with the Metropolis algorithm [24] as well as the parallel tempering (PT) method [25–27]. In the PT case, M replicas of system are simulated in parallel, each in different temperature T_i, with

*mbanasz@amu.edu.pl; http://zfwc.home.amu.edu.pl

i ranging from 1 to M. After 2×10^4 MC steps we try to exchange replicas with neighboring T_i in random order with probability

$$p(T_i \leftrightarrow T_{i+1}) = \min[1, \exp(-(\beta_i - \beta_{i+1})(U_{i+1} - U_i))], \tag{1}$$

where $\beta_i = 1/kT_i$ and U_i is potential energy of replica at T_i. This method offers efficient equilibration at low temperatures, yielding results which are significantly less noisy and which are reproducible. We updated all data every 10^3 steps and configurations every 10^5 steps (selectively 10^4 for particularly interesting regions).

We repeat the experiment at least 3 times starting with different initial configurations, in which the polymer chains assume statistical conformations and random orientations and are uniformly distributed within the simulation box. A single MC step is defined as an attempt to move a given segment. Usually, the first half of a run is used to equilibrate the system and the second one to collect the data. The results are averaged over all simulation runs. We used from 5×10^6 to 10×10^6 MC steps, with 32 to 72 replicas possessing a geometric distribution of temperatures. While the morphologies obtained in the simulations were quantitatively dependent on the box size, this dependence was weak and did not change the main conclusions qualitatively.

We use the following set of interaction energies which are limited to the nearest neighbors:

$$\epsilon_{AB} = \epsilon, \tag{2}$$

$$\epsilon_{AA} = 0, \tag{3}$$

$$\epsilon_{BB} = 0, \tag{4}$$

where ϵ is an energy unit, and we define the reduced energy per lattice site and the reduced temperature as

$$\frac{E^*}{n_a} = \frac{E/\epsilon}{n_a}, \tag{5}$$

$$T^* = \frac{kT}{\epsilon}. \tag{6}$$

On the basis of considerations presented in Ref. [28] we can relate T^* used in this paper to the Flory χ parameter employed in the self-consistent field theory [29] by the following approximate equation:

$$\chi = \frac{7.5}{T^*}. \tag{7}$$

The above equation can also be used in order to relate theoretical T^*'s to experimental χ's.

The heat capacity, C_v, is calculated from the energy fluctuations as follows:

$$\frac{C_v}{n_a} = \frac{\langle (E^* - \langle E^* \rangle)^2 \rangle}{n_a T^{*2}}. \tag{8}$$

We also calculate the structure factor $[S(k)]$ using the following equation:

$$S(\vec{k}) = \frac{1}{n_\alpha} \left\langle \left(\sum_{m=1}^{n_\alpha} \cos(\vec{k} \cdot \vec{r}_m) \right)^2 + \left(\sum_{m=1}^{n_\alpha} \sin(\vec{k} \cdot \vec{r}_m) \right)^2 \right\rangle_{\texttt{thermal average}}, \tag{9}$$

where n_α is the number of segments of type α and $\vec{r}_m$ is the position of mth segment of type α. The wave vectors $\vec{k}$ are commensurate with the simulation box size, and this constraint limits their possible lengths. The visual observation of the morphology from simulations and analysis of $S(k)$ peaks are used to identify the type of the nanostructure. The peaks in the dependence of C_v on T^* are used to determine the ODT and OOT temperatures.

Previously [13,14], we studied the $A_x B_{40} A_{40-x}$ series and $A_x B_{48} A_{48-x}$ series with $x = 1$, 2, and 3, but for this study we mostly use the $A_x B_{48} A_{48-x}$ series consisting of the following sequences: A_1-B_{48}-A_{47}, A_2-B_{48}-A_{46}, and A_3-B_{48}-A_{45}, which indicates that we have the same fraction of A and B within the chain (50:50 A:B), but the A1 block is much shorter than the A2 block. The chains are placed on the FCC $96 \times 48 \times 48$ lattice with usual boundary conditions, and at a selected parameter we take the $96 \times 96 \times 96$ and $80 \times 40 \times 40$ lattices. Those lattice sites which are not filled with triblock chains are populated with a selective homopolymer, either of type A or B. As already mentioned in the Introduction, we use two homopolymer

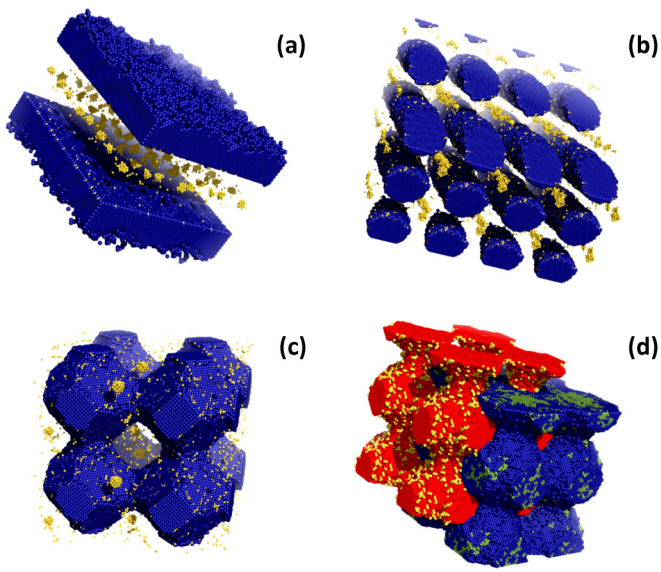

FIG. 1. Selected snapshots: (a) lamellar structure for the A_1-B_{48}-A_{47}/A blend, $\phi = 0.7$, $N_H = N_C$, $T^* = 1.0$; (b) cubically packed cylinders for the A_1-B_{48}-A_{47}/A blend, $\phi = 0.7$, $N_H = N_C/4$, $T^* = 2.5$; (c) truncated octahedra for the A_1-B_{48}-A_{47}/B blend, $\phi = 0.9$, $N_H = N_C$, $T^* = 1.3$; (d) truncated octahedra for the A_2-B_{48}-A_{46}/A blend, $\phi = 0.8$, $N_H = N_C/4$, $T^* = 3.3$. A_2 blocks are indicated in dark gray (blue in the online version), A_1-blocks in very light gray (yellow in the online version), B-blocks in medium gray (red in the online version), and A-homopolymer in light gray (green in the online version). The B-blocks and A-homopolymers are not shown in (a), (b), and (c) for clarity.

lengths, $N_H = N_C$ or $N_C/4$. The copolymer volume fraction (that is the fraction of lattice sites occupied by copolymer) is denoted by Φ. Specifically, we consider the following triblock systems: A1BA2 triblocks in the selective A homopolymer, with the $\Phi = 0.7$, $\Phi = 0.8$, and $\Phi = 0.9$ copolymer volume fractions, pure A1BA2 melt ($\Phi = 1.0$), and A1BA2 triblocks in the selective B homopolymer, with the $\Phi = 0.7$, $\Phi = 0.8$, and $\Phi = 0.9$ copolymer volume fractions.

Therefore, for the $N_H = N_C$ case we simulate the following number of copolymer chains, n_C, and homopolymer chains, n_H:

(i) For $\phi = 0.9$ we have $n_C = 1037$ and $n_H = 115$ (the $96 \times 48 \times 48$ box) and $n_C = 4147$, $n_H = 461$ (the $96 \times 96 \times 96$ box) which yields $\phi = 0.9002$ and $\phi = 0.9000$, respectively,

(ii) for $\phi = 0.8$ we have $n_C = 922$ and $n_H = 230$ (the $96 \times 48 \times 48$ box) and $n_C = 3686$, $n_H = 922$ (the $96 \times 96 \times 96$ box) which yields $\phi = 0.8003$ and $\phi = 0.7999$, respectively,

(iii) for $\phi = 0.7$ we have $n_C = 806$ and $n_H = 346$ (the $96 \times 48 \times 48$ box) and $n_C = 3226$, $n_H = 1382$ (the $96 \times 96 \times 96$ box) which yields $\phi = 0.6997$ and $\phi = 0.7001$, respectively.

For the $N_H = N_C/4$ case the number of the homopolymer chains is simply increased 4 times because we can imagine that we cut each homopolymer chain in four equal pieces.

III. RESULTS

We simulate ABA/(A or B) mixtures over a wide range of volume fraction and temperatures, but before unveiling more detailed numerical results we simply show some of the self-assembled nanostructures that form below the ODT temperature. In Fig. 1 we present representative snaphosts from the simulations of the copolymer-homopolymer blends. In particular, in Fig. 1(a) lamellar structure is shown for the A_1-B_{48}-A_{47} copolymer which is mixed with the A homopolymer ($\phi = 0.7$ and $N_H = N_C$) at $T^* = 1.0$ which is well below the ODT.

Note that the short A_1 block is shown in yellow and the long A_2 block in blue; the B blocks are not displayed in this snapshot. As expected, the A_2 blocks form ordered layers and some of the A_1 blocks locate in the B domain forming interstitial micelles as already demonstrated for both selected copolymer melts [13] and solutions [14]. Furthermore, in Fig. 1(b) cubically packed cylinders are obtained for the A_1-B_{47}-A_{46} copolymer which is mixed with the A homopolymer ($\phi = 0.7$ and $N_H = \frac{1}{4}N_C$) at $T^* = 2.5$. In the B matrix the A_2 interstitial micelles can easily be identified (in yellow). Figure 1(c) exhibits a surprising picture of ordered truncated octahedra which have been recently observed in midblock-solvated triblock copolymers [30]. The conditions for these stable octahedra occur at $T^* = 1.3$ for the A_1-B_{48}-A_{47} copolymer mixed B homopolymer ($\phi = 0.9$, $N_H = N_C$) Nanostructures possessing the truncted octahedron spatial symmetry occur in numerous inorganic systems, including natural minerals (e.g., clay, talc, and mica), mineral-organic polyhedra [31], and powder catalysts [32].

Finally, in Fig. 1(d) we also show the ordered truncated octahedra, but this time also with the B blocks (indicated in red) and A homopolymers (indicated in green). It is worthwhile

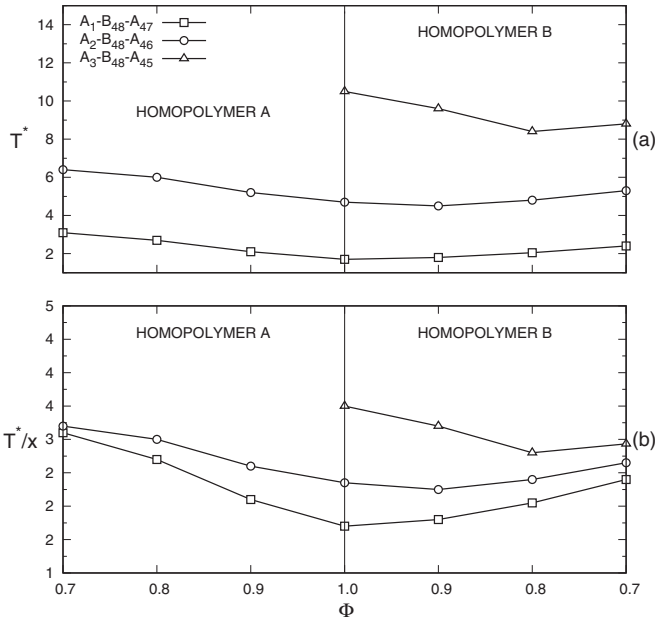

FIG. 2. (a) The interface-domain crossover temperature, T^*_{IDC}, and (b) the reduced interface-domain crossover temperature $T^*_{\mathrm{IDC}/x}$ as a function of copolymer volume fraction for the A_1BA_2/A blend (left-hand side) and the A_1BA_2/B blend (right-hand side) for $N_H = N_C/4$. The A_1-B_{48}-A_{47} triblock is indicated by open squares, the A_2-B_{48}-A_{46} triblock by open circles, and the A_3-B_{48}-A_{45} triblock by open triangles; $x = 1,2$, or 3.

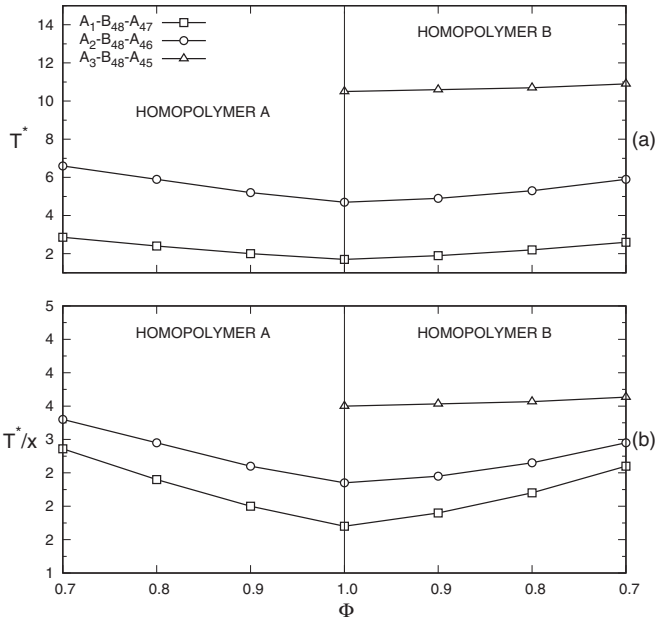

FIG. 3. (a) The interface-domain crossover temperature, T^*_{IDC}, and (b) the reduced interface-domain crossover temperature $T^*_{\mathrm{IDC}/x}$ as a function of copolymer volume fraction for the A_1BA_2/A blend (left-hand side) and the A_1BA_2/B blend (right-hand side) for $N_H = N_C$. The A_1-B_{48}-A_{47} triblock is indicated by open squares, the A_2-B_{48}-A_{46} triblock by open circles, and the A_3-B_{48}-A_{45} triblock by open triangles; $x = 1,2$, or 3.

to notice that the B blocks form the complementary network of truncated octahedra. This intriguing nanostructure is obtained for the A_2-B_{48}-A_{46} copolymer mixed with A homopolymer ($\phi = 0.8$, and $N_H = N_C/4$) at $T^* = 3.3$.

The temperature at which the short A_1 blocks are equally distributed into the interface and the B-domain can be identified as the interface-domain crossover (IDC) temperature, $T^*_{\rm IDC}$, as defined in Ref. [14]. Thus, below this temperature most A_1 blocks are localized in the B-domain which may further lead into the interstitial micelles formation. For pure melts ($\Phi = 1$) the $T^*_{\rm IDC}$ increases with increasing the short A block, as indicated in Figs. 2 and 3 for the 1–48–47, 2–48–46, and 3–48–45 triblock chains. It is also worthwhile to notice that the $T^*_{\rm IDC}$ mostly increases with the increasing total fraction of homopolymer (either A or B). This trend will continue for the interstitial micelles formation as homopolymer is added (see Figs. 5 and 6). It is interesting that the results for the $N_H = N_C/4$ blend (Fig. 2) and for the $N_H = N_C$ blend (Fig. 3) are similar, indicating a weak dependence of the $T^*_{\rm IDC}$ on the homopolymer length. In Figs. 2(b) and 3(b), on the other hand, we show the reduced interface-domain crossover temperatures,

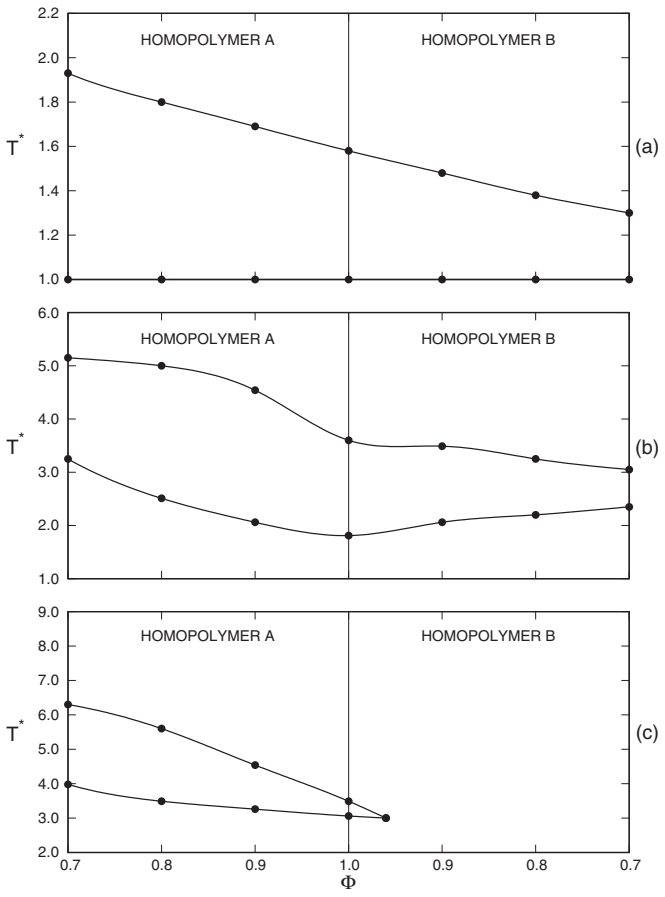

FIG. 4. Region of stability of the interstitial micelles for the copolymer-homopolymer blend for $N_H = N_C/4$. This region lies between the solid lines which are shown as a function of copolymer volume fraction, ϕ, in a selective A homopolymer and B homopolymer and the reduced temperature T^* (pure melt is at $\phi = 1$). Panel figures refer to the following A_1BA_2 triblock copolymer blends: (a) A_1-B_{48}-A_{47}, (b) A_2-B_{48}-A_{46}, and (c) A_3-B_{48}-A_{45}.

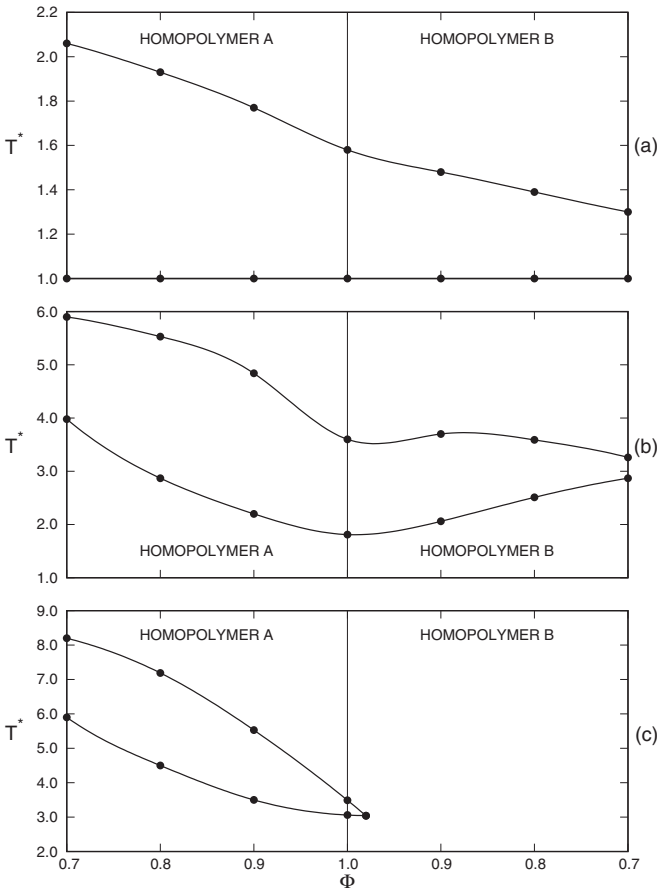

FIG. 5. Region of stability of the interstitial micelles for the copolymer-homopolymer blend for $N_H = N_C$. This region lies between the solid lines which are shown as a function of copolymer volume fraction, ϕ, in a selective A homopolymer and B homopolymer and the reduced temperature T^* (pure melt is at $\phi = 1$). Panel figures refer to the following A_1BA_2 triblock copolymer blends: (a) A_1-B_{48}-A_{47}, (b) A_2-B_{48}-A_{46}, and (c) A_3-B_{48}-A_{45}.

$T^*_{\rm IDC}/x$, for the x-48-(48-x) series ($x = 1, 2, 3$), illustrating the extent to which curves of Figs. 2(a) and 3(a) collapse when divided by the length of the short A block.

In Figs. 4 ($N_H = N_C/4$) and 5 ($N_H = N_C$) we show the regions of stability for the IM's which are the areas between solid lines (or below the solid line if only one line can be seen) shown in the (T^*, Φ) phase diagrams for different triblock-homopolymer blends. It is worthwhile to notice that if the A homopolymer is added the solution contains more segments of type A, whereas if the B homopolymer is added the segments of type B are in majority. We observe for both homopolymers that the temperature at which the IM's are formed (upper solid line) increases as A homopolymer is added and decreases as the B homopolymer is added. This is similar to that of the corresponding selective solvents of type A and B, as demonstrated earlier [14]. Also the results for the $N_H = N_C/4$ blend (Fig. 4) and for the $N_H = N_C$ blend (Fig. 5) are similar, indicating a weak dependence of the $T^*_{\rm IDC}$ on the IM stability regions.

While Figs. 4 and 5 exhibit exclusively the stability regions for the IM's, in Figs. 6 ($N_H = N_C/4$) and 7 ($N_H = N_C$) we

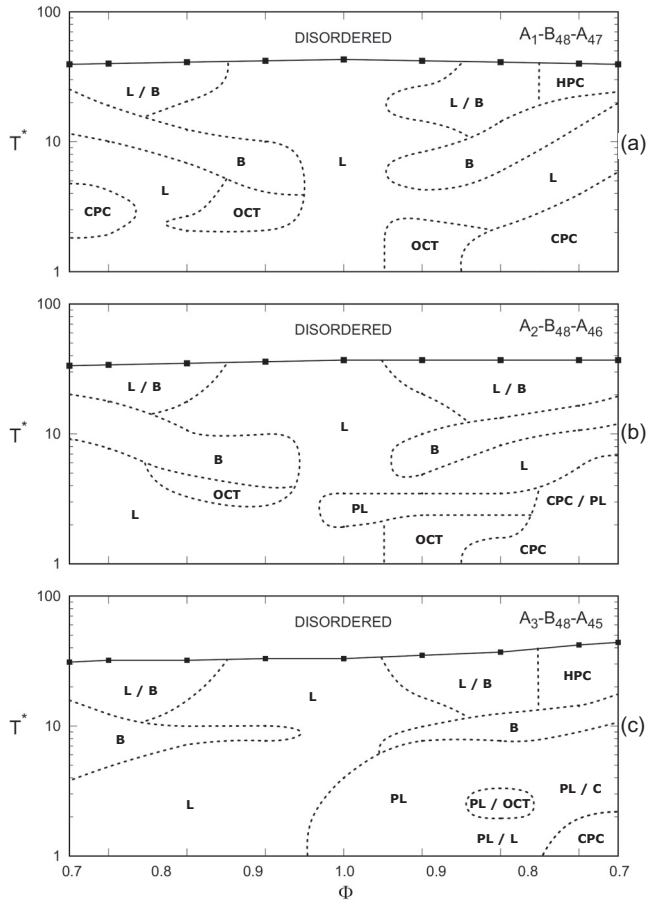

FIG. 6. Phase diagrams as a function of a triblock copolymer volume fraction and temperature in a selective homopolymer of either type A (on the left-hand side) or type B (on the right-hand side) and the temperature T^* for $N_H = N_C/4$. Panel figures refer to the following triblock chains: (a) A_1-B_{48}-A_{47}, (b) A_2-B_{48}-A_{46}, and (c) A_3-B_{48}-A_{45}. Order-disorder and order-order lines are shown as solid and dashed lines, respectively.

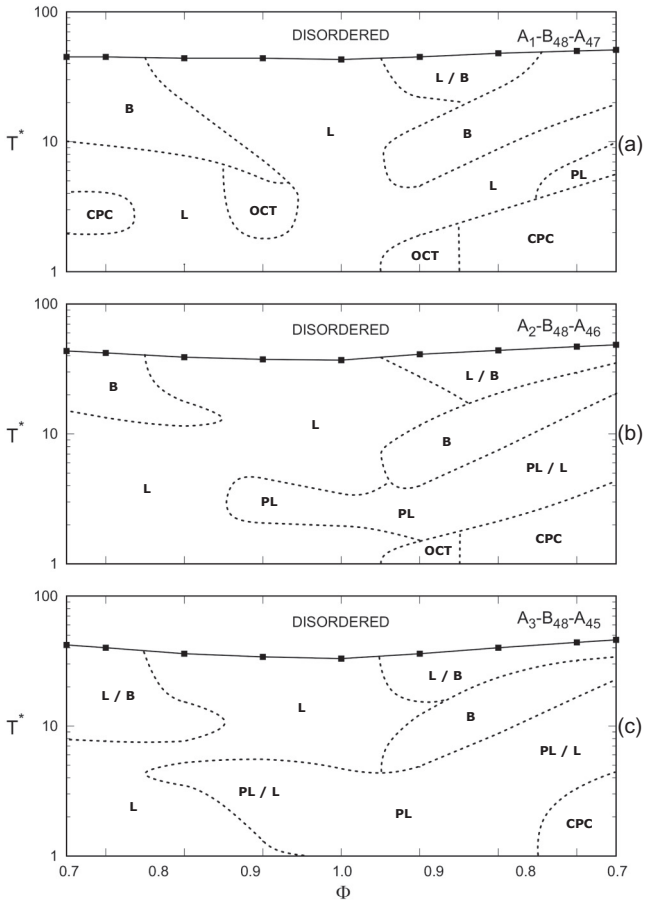

FIG. 7. Phase diagrams as a function of a triblock copolymer volume fraction and temperature in a selective homopolymer of either type A (on the left-hand side) or type B (on the right-hand side) and the temperature T^* for $N_H = N_C$. Panel figures refer to the following triblock chains: (a) A_1-B_{48}-A_{47}, (b) A_2-B_{48}-A_{46}, and (c) A_3-B_{48}-A_{45}. Order-disorder and order-order lines are shown as solid and dashed lines, respectively.

also show the ODT lines and indicate the type of nanostructure in the (T^*, Φ) plane for the x-48-(48-x) series. For clarity of the presentation we use the logarithmic scale on the T^* axis. We observe the following nanostructures: layers (L), hexagonally packed cylinders (HPC), cubically packed cylinders (CPC), perforated layers (PL), gyroid or double diamond bicontinuous nanostructure (B), and ordered truncated octahedra (OCT). We also observe phase regions, where more than one nanostructure is recorded simultaneously(marked with a slash, e.g., L/B). While there are significant differences for various homopolymer lengths ($N_H = N_C/4$ vs. $N_H = N_C$), the general features for both cases are remarkably similar. It is also evident that significant difference in the structural assemblies occur for slightly different sequences. As indicated previously, this can be explained by the fact that only the short A blocks locate in the B-matrix due to an entropic advantage over the small enthalpic penalty. This penalty is small only when the A1 block is short which, in our case, means that the A1 block can consist of one, two, or three segments. That implies that significant changes in structure occur when the number of A1 segments is increased from one to two or from two to three.

As an additional result, in Fig. 8 we show the looping fraction, f_L, as a function of the reduced temperature, T^*, for the A_1-B_{48}-A_{47}/A blend (the $N_H = N_C$ case). We clearly see

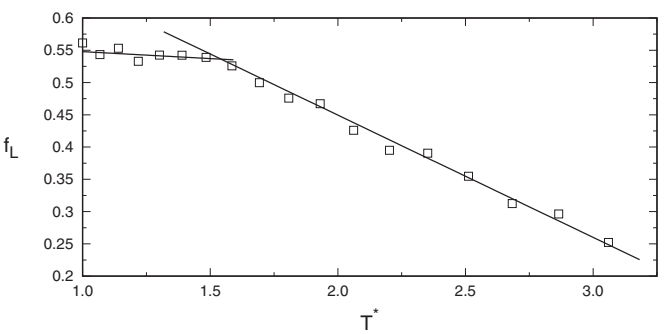

FIG. 8. Looping fraction as a function of the reduced temperature, T^*, for A_1-B_{48}-A_{47}/A blend for $N_H = N_C$).

two different regimes of behavior for the looping fraction, as the temperature is lowered. First the looping fraction increases with decreasing temperature, but then at about $T^* = 1.7$ we can observe that is stabilized at about $f_L = 0.55$. This temperature corresponds to the IM formation which indicates that IM's cannot increase f_L on cooling.

Finally, we do not observe any indications of macrophase separation. This is reminiscent of the fact that solutions of symmetric block copolymers are known to be stable [12,33,34] (even at very strong segregation regime) with respect to macrophase separation for Φ's which are greater than 0.5., and a transition to disordered micellar solution is observed for Φ's which are smaller than approximately 0.2 [12] (note that $\Phi = 0.2$ is well beyond the scope of this study).

IV. CONCLUSION

In summary, we simulated selective A1BA2/A and A1BA2/B triblock homopolymer blends using a Monte Carlo lattice method. The spatially ordered interstitial micelles were formed from the minority A1 blocks within the B block domain as a result of an entropic effect. We investigate the stability of the IM's as a function of triblock volume fraction in selective homopolymer of either type A or type B. We found that adding selective homopolymer of type A shifts the stability of the IM's into significantly higher temperatures which may provide a pathway towards experimental studies of interstitial micelles in real triblock solutions, such as, for example, polystyrene-polyisoprene-polystyrene triblock. We also found that adding selective homopolymer (either A or B) gives rise a to more complex phase behavior with the nanodomains ordered into a variety of nonlamellar nanostructures such as the ordered truncated octahedra. Finally, the phase behavior of the triblock-homopolymer blends depends relatively weakly on the chain length of the added homopolymer.

ACKNOWLEDGMENTS

Grant No. 2012/07/B/ST5/00647 of the National Science Centre (Poland) is gratefully acknowledged. A significant part of the simulations was performed at the Poznan Computer and Networking Center (PCSS). We also acknowledge fruitful discussions with Professor Richard Spontak and Dr. Kenny Mineart.

[1] I. W. Hamley, *The Physics of Block Copolymers* (Oxford University Press, New York, 1998).
[2] I. W. Hamley, *Developments in Block Copolymer Science and Technology* (John Wiley & Sons, New York, 2004).
[3] R. B. Thompson, V. V. Ginzburg, M. W. Matsen, and A. C. Balazs, Science **292**, 2469 (2001).
[4] F. S. Bates, M. A. Hillmyer, T. P. Lodge, C. M. Bates, K. T. Delaney, and G. H. Fredrickson, Science **336**, 434 (2012).
[5] L. Wu, T. Lodge, and F. Bates, Macromolecules **37**, 8184 (2004).
[6] T. Lodge, Macromol. Chem. Phys. **204**, 265 (2003).
[7] J. Lee, N. Balsara, A. Chakraborty, R. Krishnamoorti, and B. Hammouda, Macromolecules **35**, 7748 (2002).
[8] J. Wang, M. Müller, and Z.-G. Wang, J. Chem. Phys. **130**, 154902 (2009).
[9] C. Zhou, M. Hillmyer, and T. Lodge, Macromolecules **44**, 1635 (2011).
[10] K. Hanley, T. Lodge, and C.-I. Huang, Macromolecules **33**, 5918 (2000).
[11] F. Detcheverry, D. Pike, P. Nealey, M. Müller, and J. De Pablo, Phys. Rev. Lett. **102**, 197801 (2009).
[12] T. Lodge, B. Pudil, and K. Hanley, Macromolecules **35**, 4707 (2002).
[13] S. Wołoszczuk, K. P. Mineart, R. J. Spontak, and M. Banaszak, Phys. Rev. E **91**, 010601 (2015).
[14] J. E. Moisio, J. Piili, and R. P. Linna, Phys. Rev. E **94**, 022501 (2016).
[15] M. W. Matsen and R. B. Thompson, J. Chem. Phys. **111**, 7139 (1999).
[16] A. Gauger, A. Weyersberg, and T. Pakula, Die Makromolekulare Chemie, Theory and Simulations **2**, 531 (1993).
[17] A. Weyersberg and T. A. Vilgis, Phys. Rev. E **48**, 377 (1993).
[18] T. Pakula, K. Karatasos, S. H. Anastasiadis, and G. Fytas, Macromolecules **30**, 8463 (1997).
[19] T. Pakula, in *Simulation Methods for Polymers*, edited by M. J. Kotelyanskii and D. N. Thedorou (Marcel-Dekker, New York, 2004), chap. 5.
[20] M. Banaszak, S. Wołoszczuk, T. Pakula, and S. Jurga, Phys. Rev. E **66**, 031804 (2002).
[21] S. Wołoszczuk, M. Banaszak, S. Jurga, T. Pakula, and M. Radosz, J. Chem. Phys. **121**, 12044 (2004).
[22] M. Banaszak and J. Krajniak, Comput. Methods Sci. Technol. **19**, 137 (2013).
[23] K. Lewandowski, P. Knychala, and M. Banaszak, Phys. Status Solidi B **245**, 2524 (2008).
[24] N. Metropolis, A. W. Rosenbluth, M. N. Rosenbluth, A. H. Teller, and E. Teller, J. Chem. Phys. **21**, 1087 (1953).
[25] R. H. Swendsen and J. S. Wang, Phys. Rev. Lett. **57**, 2607 (1986).
[26] D. J. Earl and M. W. Deem, Phys. Chem. Chem. Phys. **7**, 3910 (2005).
[27] A. Sikorski, Macromolecules **35**, 7132 (2002).
[28] P. Knychała, M. Dzięcielski, M. Banaszak, and N. P. Balsara, Macromolecules **46**, 5724 (2013).
[29] G. Fredrickson, *The Equilibrium Theory of Inhomogeneous Polymers* (Oxford University Press, Oxford, 2007).
[30] S. Woloszczuk, M. Tuhin, S. Gade, M. Pasquinelli, M. Banaszak, and R. Spontak, ACS Appl. Mater. Interfaces **9**, 39940 (2017).
[31] D. J. Tranchemontagne, Z. Ni, M. O'Keeffe, and O. M. Yaghi, Angew. Chem., Int. Ed. **47**, 5136 (2008).
[32] W. Huang, Acc. Chem. Res. **49**, 520 (2016).
[33] M. Banaszak and M. Whitmore, Macromolecules **25**, 3406 (1992).
[34] S. Woloszczuk, M. Banaszak, P. Knychala, and M. Radosz, Macromolecules **41**, 5945 (2008).